Dalton Transactions

ROYAL SOCIETY OF CHEMISTRY

PAPER

View Article Online
View Journal | View Issue

Open Access Article. Published on 17 July 2025. Downloaded on 11/16/2025 12:52:30 AM.
This article is licensed under a Creative Commons Attribution-NonCommercial 3.0 Unported Licence.

Check for updates

Cite this: *Dalton Trans.*, 2025, **54**, 12471

Intramolecular sensitization and structure of a Tb^{3+}/2-hydroxyquinoline conjugate in the paraoxonase 1 active site†

Janez Smerkolj,[a] Miha Bahun,[b] Nataša Poklar Ulrih,[b] Aljoša Bavec,[a] Miha Pavšič[c] and Marko Goličnik *[a]

Received 24th June 2025,
Accepted 16th July 2025

DOI: 10.1039/d5dt01484k

rsc.li/dalton

Paraoxonase 1 (PON1) is a Ca^{2+}-dependent enzyme involved in oxidative stress processes and is widely studied for its protective roles in various diseases. Intermolecular sensitization of lanthanide ions was implemented by replacing Ca^{2+} ions from the recombinant PON1 (rePON1) catalytic site in the presence of 2-hydroxyquinoline (2HQ) as an external antenna. Although the replacement of Ca^{2+} ions with lanthanide ions indicates weaker binding affinity for the coordination of 2HQ in the protein milieu of the rePON1 active site, it results in the formation of a highly emissive supramolecular complex in the case of Tb^{3+} ions. The architecture of the ternary rePON1 : Tb^{3+} : 2HQ conjugate, which allows efficient terbium sensitization and its specific long-wavelength metal phosphorescence emission, was resolved by X-ray crystallography. These findings could establish a non-catalytic quantification strategy for PON1 and provide additional structural insights into lanthanide substitution in this Ca^{2+}-dependent enzyme.

Introduction

Paraoxonases (PONs) are a family of mammalian calcium (Ca^{2+})-dependent hydrolases encoded by three genes (*PON1*, *PON2*, and *PON3*).[1] These genes share approximately 70% identity in nucleotide sequences and 60% identity in amino acid sequences. Among them, PON2 is an intracellular enzyme and evolutionarily the most ancient member of the PON family.[1] Although PON2 has been detected in various tissues, PON1 and PON3 are primarily synthesized in the liver and subsequently secreted into the bloodstream, where they associate with high-density lipoproteins (HDLs).[1,2] PON1 is the most studied among the paraoxonases and is anchored to HDLs with hydrophobic regions located on its surface.[3]

Although PON1 was initially recognized for its ability to hydrolyze phosphotriesters such as paraoxon, this organophosphate hydrolysis most likely reflects its promiscuous activity rather than its primary function. In addition to phosphotriesterase activity, PON1 also acts as arylesterase and lactonase.[2] This versatility is attributed to the considerable plasticity of its catalytic site.[4–7] Conversely, PON2 and PON3 primarily exhibit lactonase activity.[8] Notably, lactonase activity is also believed to be the native activity of PON1, particularly with γ- and δ-lactones as substrates,[9] as the hydrolysis rates of aryl esters and phosphotriesters by PON1 are significantly slower.

PON1 is responsible for the antioxidative properties of HDLs,[10] and it not only protects HDL particles from oxidation but also inhibits lipid peroxidation.[11] Given its critical role in both preventing lipid peroxidation during oxidative stress and hydrolyzing oxidized lipids, PON1 is of particular interest in clinical research, particularly in the pathophysiology of cardiovascular,[11,12] neurological,[13,14] pulmonary,[15] and chronic kidney[16] diseases. Additionally, studies have reported an association between PON1 activity and cancer,[17] diabetes mellitus,[18] and non-alcoholic fatty liver disease,[19] although the exact biochemical mechanism for the putative antioxidative function of PON1 remains unclear.

Due to its hydrophobic properties, human PON1 cannot be easily isolated, purified, and crystallized for 3D structure determination. To overcome this limitation, directed evolution has been employed to shuffle various mammalian PON1 genes, resulting in chimeric recombinant PON1 (rePON1) that can be expressed in a soluble and active form in *E. coli*.[20] Structural studies of rePON1 revealed that it adopts a six-bladed β-propeller with a centrally located active site.[4,21,22] Human PON1 is well mimicked by rePON1, which shares nearly 90% sequence identity and exhibits almost identical kinetic

[a]*University of Ljubljana, Faculty of Medicine, Institute of Biochemistry and Molecular Genetics, Vrazov trg 2, 1000 Ljubljana, Slovenia. E-mail: marko.golicnik@mf.uni-lj.si*
[b]*University of Ljubljana, Biotechnical Faculty, Department of Food Science and Technology, Jamnikarjeva 101, 1000 Ljubljana, Slovenia*
[c]*University of Ljubljana, Faculty of Chemistry and Chemical Technology, Department of Chemistry and Biochemistry, Večna pot 113, 1000 Ljubljana, Slovenia*

† Electronic supplementary information (ESI) available. See DOI: https://doi.org/10.1039/d5dt01484k

Open Access Article. Published on 17 July 2025. Downloaded on 11/16/2025 12:52:30 AM.
This article is licensed under a Creative Commons Attribution-NonCommercial 3.0 Unported Licence.

parameters across various substrates.[9,20] Two Ca^{2+} ions are chelated within the rePON1 protein milieu. The first (so-called catalytic) Ca^{2+} ion, positioned near the surface of the active site, is believed to play a key catalytic role in orienting the substrate and stabilizing the negative charge of the transition state. The second (so-called structural) Ca^{2+} ion is embedded at the bottom of the catalytic cavity, where it stabilizes the catalytic conformation of the enzyme. This structural Ca^{2+} ion exhibits an affinity for its binding site up to two orders of magnitude higher than that of the catalytic Ca^{2+} ion and is essential for maintaining PON1 activity.[22–24]

The dissociation of Ca^{2+} (influenced by chelating agents such as EDTA) can inhibit the enzymatic activity of PON1.[25] Divalent metal ions can also replace native Ca^{2+} at the active site of PON1. *In vitro* studies have shown that certain divalent metal ions exhibit an inhibitory effect on PON1 activity.[22,26] The putative mechanism of PON1 inhibition by these metal ions involves their binding to different amino acid residues.[27] However, although most metal ions can inhibit PON1 activity, reactivation of PON1 can typically be achieved by adding excess Ca^{2+}.

Rare earth metals are among the most potent metal inhibitors of PON1; however, their binding interactions with PON1 have rarely been studied.[26,28] This is interesting because several lanthanides are isomorphous with Ca^{2+}, making them useful probes for Ca^{2+} binding to proteins in structural studies.[29] In addition to their role in structural analyses, lanthanides owing to their privileged and uniquely specific phosphorescence emissive properties have been used in the formation of biosensing lanthanide supramolecular complexes.[30,31] However, this phenomenon in the context of PON1 has only been reported by Josse *et al.*, who demonstrated that the displacement of calcium (Ca^{2+}) ions with terbium (Tb^{3+}) ions resulted in the formation of a weakly emissive PON1 : Tb^{3+} complex with a specific characteristic metal spectrum profile.[24]

Therefore, we aimed to investigate the potential spectroscopic properties of a ternary complex involving rePON1, its known aromatic competitive inhibitor (2-hydroxyquinoline – 2HQ), and lanthanide ions (Ln^{3+}). Various hydroxyquinolines are commonly used as antenna molecules in photoluminescent Ln^{3+} chelates.[32–35] These compounds exhibit two characteristic absorbance peaks (270 and 324 nm) in the UV spectrum, enabling them to act as efficient UV light sensitizers at wavelengths beyond the absorbance range of aromatic amino acid residues. The characterization and detection of PON1 active sites through intermolecular sensitization of the ternary complex PON1 : Ln^{3+} : 2HQ might also serve as a useful approach for determining enzyme concentrations in biological samples.

Results and discussion

Experimental techniques

Expression and purification of rePON1 were performed as previously described,[20–22] with certain changes. Rosetta-gami B(DE3) *E. coli* pLysS cells, transformed with plasmid pET32b (+)-rePON1-G2E6, were used for the rePON1 expression. Protein precipitation, Ni affinity and ion-exchange chromatography were carried out for the purification of rePON1 from cell lysates. Protein cleavage was performed afterwards due to rePON1 expression as a fusion protein with thioredoxin, and for crystallization, the protein was subjected to additional ion-exchange and size-exclusion chromatography.

Most spectroscopic characterization studies for detecting the formation of the ternary complexes rePON1 : Ln^{3+} : 2HQ were carried out in bis-tris-propane (BTP) buffer solutions (pH 7.4), supplemented with certain concentrations of metal ions and 2HQ. Stability of the rePON1 : Tb^{3+} : 2HQ complex was assessed under a series of various buffer and pH conditions. Isothermal titration calorimetry (ITC) was used to investigate the binding interaction between 2HQ and rePON1 in either its Ca^{2+}- or Tb^{3+}-bound form in HEPES buffer (pH 8.0). The thermal stabilities of rePON1 : Ca^{2+} : 2HQ and rePON1 : Tb^{3+} complexes were assessed using nano-differential scanning fluorimetry in BTP (pH 7.4 and 8.0).

Crystals of the rePON1 : Tb^{3+} : 2HQ complex were obtained using the sitting-drop vapor diffusion method. When rod-shaped crystals appeared, they were harvested, cryoprotected and flash-frozen in liquid nitrogen. X-ray diffraction data were collected at the XRD2 beamline of the Elettra Synchrotron (Trieste, Italy).

All other details on experimental techniques and conditions can be found in the ESI.†

Spectra of the rePON1 : Ln^{3+} : 2HQ complexes

To establish the feasibility of using lanthanide metal-specific phosphorescence spectroscopy for the quantification of rePON1, we recorded the emission spectra of the ternary rePON1 : Tb^{3+} : 2HQ complex and compared them to those of other lanthanide ion (Ln^{3+}) complexes. The spectra were recorded using an excitation wavelength of 351 nm and measured over a wavelength range of 400–700 nm.

A variety of emission colors in the visible spectra can be expected using different Ln^{3+} complexes. Sm^{3+}, Eu^{3+}, Dy^{3+}, Tb^{3+}, and Tm^{3+} tris(β-diketonates) emit in the orange, red, yellow, green, and blue regions of visible light, respectively,[31] but other Ln^{3+} complexes emit in the near-infrared region.

The Tb^{3+}-containing ternary complex exhibited the strongest emission, characterized by distinct emission peaks at 491 nm, 545 nm, 588 nm, and 621 nm (Fig. 1, green solid line).

These peaks correspond to the characteristic f–f transitions of Tb^{3+} ($^5D_4 \rightarrow {}^7F_6$, $^5D_4 \rightarrow {}^7F_5$, $^5D_4 \rightarrow {}^7F_4$, and $^5D_4 \rightarrow {}^7F_3$, respectively).[36] Additionally, this emission profile confirms an efficient antenna ligand-to-Tb^{3+} energy transfer within the rePON1 : Tb^{3+} : 2HQ complex. The most intense emission at 545 nm, corresponding to the $^5D_4 \rightarrow {}^7F_4$ transition of Tb^{3+}, indicates the formation of a stable and well-coordinated phosphorescent complex.

In the remaining lanthanide ions, we expected to detect a signal under our experimental conditions from those that emit light in the visible spectrum, such as Sm^{3+}, Eu^{3+}, Dy^{3+}, and

 This journal is © The Royal Society of Chemistry 2025

Open Access Article. Published on 17 July 2025. Downloaded on 11/16/2025 12:52:30 AM.
This article is licensed under a Creative Commons Attribution-NonCommercial 3.0 Unported Licence.

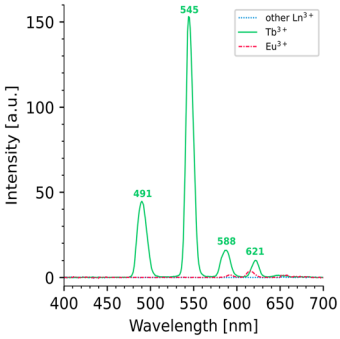

Fig. 1 Phosphorescence emission spectra of the rePON1 : Tb^{3+} : 2HQ complex compared to those of other lanthanide (Ln^{3+})-containing complexes in 20 mM bis-tris-propane buffer at pH 7.4. Final concentrations of rePON1 were 1 μM for Tb^{3+} ions and 2 μM for other Ln^{3+} ions, along with a 50 μM concentration of lanthanide ions and 400 μM 2HQ. The green solid line represents the emission spectra of the Tb^{3+}-containing ternary complex, exhibiting distinct Tb^{3+}-characteristic emission signal peaks. The red dash-dotted line represents the emission spectra of the Eu^{3+}-containing ternary complex, exhibiting weak but distinct peaks at 591 nm and 615 nm. Complexes containing other Ln^{3+} ions (blue dotted line) display negligible emission under the same experimental conditions.

Tm^{3+}. Among these, Eu^{3+} is particularly well-known and frequently used as a luminescent probe. As expected, no phosphorescence was observed with other Ln^{3+} ions, which characteristically emit in the near-infrared spectrum.

Only the Eu^{3+}-containing ternary complex (red dash-dotted line in Fig. 1) exhibited weak emission, with two minor peaks at 591 nm and 615 nm, corresponding to the $^5D_0 \rightarrow {}^7F_1$ and $^5D_0 \rightarrow {}^7F_2$ transitions of Eu^{3+}, respectively.[36] The faint emission of Eu^{3+} suggests that its phosphorescence is limited either by inefficient energy transfer from 2HQ to Eu^{3+} or by weak and poorly coordinated complex formation with rePON1.[37] It should be noted that phosphorescent Ln^{3+} probes, such as Tb^{3+} and Eu^{3+}, are highly sensitive to their local environment, as their decay times depend on the number of coordinated water molecules.[38] Therefore, lifetime measurements of Tb^{3+}/Eu^{3+} upon Ca^{2+} replacement within protein structures can serve as a proxy for determining the hydration states of protein-bound metal ions. Another well-known phosphorescence deactivation pathway for the excited states of lanthanide ions involves vibrational energy transfer of high-energy oscillators, particularly OH (typically from bound water molecules), NH (from amide and amine groups), and CH bonds.[38,39] Among these, water molecules are the most efficient quenchers, both in the solid state and in solution.

It is known that compared to Tb^{3+} transitions, Eu^{3+} transitions couple more efficiently with the vibrational overtones of nearby water OH oscillators, resulting in more effective quenching. In addition, Eu^{3+} exhibits one of the slowest water exchange rates of tetraamide complexes, up to 500-fold slower[40] than that of Tb^{3+}. Collectively, these factors may explain the absence of detectable phosphorescence for several lanthanide ions, including Eu^{3+}. They also emphasize the unique photophysical behavior of the rePON1 : Tb^{3+} : 2HQ complex, particularly in terms of phosphorescence efficiency and stability, when compared to other lanthanide ion-containing systems.

Photophysical properties of 2HQ and the rePON1 : Tb^{3+} : 2HQ complex

The photophysical properties of the ternary rePON1 : Tb^{3+} : 2HQ complex were investigated by recording excitation and emission spectra. Additionally, ligand binding was assessed by comparing the absorption spectra of 2HQ and the excitation spectra of the formed ternary complex.

The excitation spectrum of the rePON1 : Tb^{3+} : 2HQ complex was recorded over a wavelength range of 250–400 nm, with emission monitored at 545 nm (Fig. 2A, green solid line). Two major excitation peaks were observed at 288 nm and 351 nm, indicating that 2HQ can effectively transfer energy to Tb^{3+} within the rePON1 : Tb^{3+} : 2HQ complex, leading to the observed emission. In contrast, the rePON1 : Tb^{3+} complex alone exhibited a weak excitation peak at 280 nm (Fig. 2A, blue dotted line), suggesting that aromatic amino acids near the bound Tb^{3+} contribute to excitation under these conditions.[41] However, the absence of a detectable emission signal at an excitation wavelength of 351 nm indicates that intrinsic aromatic residues in rePON1 are inefficient antennas for accepting and transferring energy to Tb^{3+} without 2HQ.

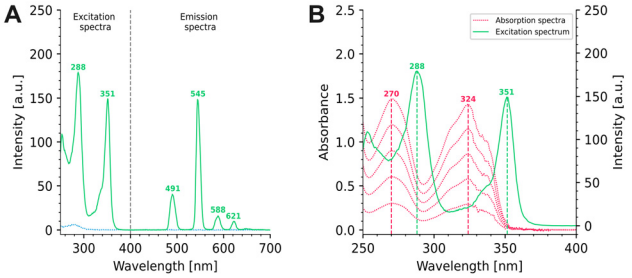

Fig. 2 Phosphorescence excitation and emission spectra of the rePON1 : Tb^{3+} : 2HQ complex in 20 mM bis-tris-propane buffer at pH 7.4 ([rePON1] = 1 μM, [Tb^{3+}] = 50 μM, and [2HQ] = 400 μM), along with the overlapping absorption spectra of 2HQ in 20 mM bis-tris-propane buffer at pH 7.4. (A) Excitation spectrum (green solid line – λ_{em} = 545 nm) showing major signal peaks at 288 nm and 351 nm. Additionally, the excitation spectrum of rePON1 : Tb^{3+} (blue dotted line – λ_{em} = 545 nm) shows a weak signal at approximately 280 nm. The emission spectrum (green solid line – λ_{ex} = 351 nm) was recorded at an excitation wavelength of 351 nm over a wavelength range of 400–700 nm, revealing distinct and Tb^{3+}-characteristic emission signal peaks. Furthermore, the emission spectra (blue dotted line – λ_{ex} = 351 nm) of rePON1 : Tb^{3+}, rePON1 : Ca^{2+}, rePON1 : Ca^{2+} : 2HQ, and Tb^{3+} : 2HQ were recorded under the same conditions, and no detectable signal peaks were observed for these complexes. (B) The absorption spectra of 50–250 μM 2HQ (red dotted lines) overlaid with the excitation spectrum of the rePON1 : Tb^{3+} : 2HQ complex (green solid line – λ_{em} = 545 nm). Although both spectra have a similar shape, the excitation spectrum is shifted to the right relative to the absorption spectra, indicating a change in the environment of 2HQ.

Open Access Article. Published on 17 July 2025. Downloaded on 11/16/2025 12:52:30 AM.
This article is licensed under a Creative Commons Attribution-NonCommercial 3.0 Unported Licence.

Furthermore, the control samples (rePON1 : Ca^{2+}, rePON1 : Ca^{2+} : 2HQ, and Tb^{3+} : 2HQ) did not produce detectable emission signals. This confirms that all three components, rePON1, Tb^{3+}, and 2HQ, are essential for the formation of a supramolecular phosphorescent complex with efficient emission. These findings support our hypothesis that 2HQ functions as an efficient external antenna ligand, facilitating ligand-to-Tb^{3+} energy transfer within the rePON1 : Tb^{3+} : 2HQ complex, ultimately leading to its characteristic metal emission spectrum.

Fig. 2B compares the absorption spectra of 2HQ at five different concentrations (50, 100, 150, 200, and 250 μM) with the excitation spectrum of the rePON1 : Tb^{3+} : 2HQ complex. The absorption spectrum of free 2HQ displays two peaks at 270 nm and 324 nm, consistent with previously reported values.[42] A key observation is that the excitation spectrum of the rePON1 : Tb^{3+} : 2HQ complex closely mirrors the shape of the 2HQ absorption spectra but is red-shifted by 18 nm and 27 nm at the respective peaks. It is well established that the absorption maxima shift to longer wavelengths as the electron density around the ligand increases.[43] Such shifts may result from coordination to a metal ion or changes in solvent polarity, such as upon protein binding. Therefore, the observed red shift suggests that 2HQ effectively binds with the complex, and the altered excitation profile reflects changes in its electronic environment upon complex formation.

Additionally, the absence of emission in the other complexes (rePON1 : Ca^{2+}, rePON1 : Ca^{2+} : 2HQ, and Tb^{3+} : 2HQ) suggests that only the rePON1 active site provides a specific protein milieu for conjugate formation that enables intermolecular sensitization of Tb^{3+} by the aromatic ligand 2HQ acting as an external antenna.

2HQ- and Tb^{3+}-dependent formation of the rePON1 : Tb^{3+} : 2HQ complex

The binding interaction of 2HQ with rePON1 : Ca^{2+} and rePON1 : Tb^{3+} was assessed using ITC (Fig. SI1†). Binding isotherms were globally fitted using a 1 : 1 binding model in SEDPHAT. For rePON1 : Ca^{2+} (Fig. SI1A†), analysis of the thermogram yielded a binding affinity of $\log_{10} K_A$ = 5.657 (CI: 5.551–5.763), corresponding to K_D = 2.20 μM (CI: 1.73–2.81 μM). These values are consistent with previously reported data.[4] The interaction was strongly exothermic (ΔH = −7.382 kcal mol^{-1}) and accompanied by positive entropy (ΔS = 1.126 cal/molK), indicating an enthalpy-driven interaction (ΔG = −7.718 kcal mol^{-1}). In contrast, rePON1 : Tb^{3+} (Fig. SI1B†) exhibited significantly decreased affinity for 2HQ (estimated for more than 20-fold decrease), and thus no clear transition in the binding isotherm was observed.

Notably, phosphorescence spectroscopy conducted on the same dialyzed sample confirmed that 2HQ binds to the rePON1 : Tb^{3+} complex, forming an emissive rePON1 : Tb^{3+} : 2HQ complex, as indicated by the characteristic emission spectrum like the one presented in Fig. 1. This indicates that 2HQ effectively binds to the rePON1 : Tb^{3+} complex, albeit with decreased affinity compared to the rePON1 : Ca^{2+} complex. However, the binding affinity experiments could not be performed with high precision due to the limitations of the ITC methodological approach. Accurate quantification of weak binding would require higher concentrations of rePON1 and Tb^{3+}, which may lead to protein aggregation.

Following our ITC results, which indicated weaker binding of 2HQ to the rePON1 : Tb^{3+} complex, we further characterized the interaction by performing phosphorescence titrations. Specifically, a series of solutions were prepared with varying 2HQ concentrations (0.5–1000 μM), while maintaining fixed concentrations of rePON1, Ca^{2+}, and Tb^{3+} at 1 μM, 13.3 μM, and 50 μM, respectively (Fig. 3A). The emission intensity was monitored as a function of ligand concentration to assess binding behavior. In a separate experiment, we examined the effect of Tb^{3+} concentration on complex stability and phosphorescence efficiency by preparing a series of Tb^{3+} concentrations (0.1–250 μM), while maintaining the rePON1, Ca^{2+}, and 2HQ concentrations constant at 1 μM, 13.3 μM, and 400 μM, respectively (Fig. 3B).

Fig. 3A shows the emission intensity (peak area at 545 nm) as a function of increasing 2HQ concentrations. The intensity initially increases with increasing 2HQ concentrations, reaching a maximum at approximately 250 μM 2HQ, and then slightly decreases at higher 2HQ concentrations. A similar trend, including phosphorescence quenching at elevated 2HQ levels, was also observed at pH 8.0 (Fig. SI2A†). Such complex titration profiles are frequently observed with lanthanide complexes. Thus, they are well-described by a fitted 1 : 1 P + L ⇌ PL and 1 : 2 PL + L ⇌ PL2 mixed binding model,[44] which assumes sequential binding of two 2HQ molecules to the complex (Table 1).

The first binding event, characterized by a dissociation constant (K_{D1}) of approximately 77 μM, is associated with a strong ligand-to-Tb^{3+} energy transfer, thereby enhancing emission

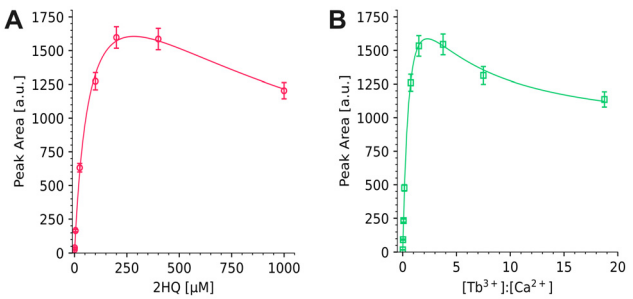

Fig. 3 The effects of 2HQ concentration (A) and the [Tb^{3+}] : [Ca^{2+}] ratio (B) on the emission intensity of the rePON1 : Tb^{3+} : 2HQ complex in 20 mM bis-tris-propane buffer at pH 7.4. (A) The peak area of emission signal intensity at 545 nm plotted against 2HQ concentrations (red circles), while maintaining rePON1 (1 μM), Ca^{2+} (13.3 μM), and Tb^{3+} (50 μM) concentrations fixed, along with a fitted curve (red solid line) based on a 1 : 1 and 1 : 2 mixed binding model. (B) The peak area of emission signal intensity at 545 nm plotted against [Tb^{3+}] : [Ca^{2+}] ratios (green squares), while maintaining rePON1 (1 μM), Ca^{2+} (13.3 μM), and 2HQ (400 μM) concentrations fixed, along with a fitted curve (green solid line) based on a 1 : 1 and 1 : 2 mixed binding model.

Open Access Article. Published on 17 July 2025. Downloaded on 11/16/2025 12:52:30 AM.
This article is licensed under a Creative Commons Attribution-NonCommercial 3.0 Unported Licence.

Table 1 Binding parameters obtained by fitting the mixed binding model (1 : 1 and 1 : 2) to the titration profiles shown in Fig. 3

Parameter	Values for 2HQ	Values for Tb^{3+}
K_{D1}	76.9 μM (1 ± 0.12)	8.3 μM (1 ± 0.14)
K_{D2}	1040 μM (1 ± 0.13)	47 μM (1 ± 0.29)

intensity. This enhancement likely results from the effective coordination of 2HQ to Tb^{3+} within the rePON1 : Tb^{3+} : 2HQ complex, which stabilizes the excited state of Tb^{3+} and facilitates efficient ligand-to-Tb^{3+} energy transfer. The evaluated affinity of 2HQ for rePON1 : Tb^{3+} is consistent with the ITC data, further supporting the observation that the binding of 2HQ to rePON1 : Tb^{3+} is weaker than that to rePON1 : Ca^{2+}. This also explains why the binding constant could not be accurately determined using ITC, as the measured K_D value falls within a range in which the heat change upon binding is too low to be reliably detected by calorimetric methods. Instead, the emission-based approach provides an indirect but effective means of assessing ligand binding.

2HQ, a weak base in its electronic ground state, is known to exist in two tautomeric forms: lactim (2-quinolinol) and lactam (2-quinolinone). The solvated lactam form is stabilized by a zwitterionic resonance structure. In this zwitterion, nitrogen carries a positive charge and single-bonded oxygen carries a negative charge. Polar solvents such as water should stabilize this zwitterionic resonance form and decrease the energy of lactam relative to the lactim tautomer (the lactam form is considered more stable by ~5 kcal mol^{-1} in aqueous solutions[45]). However, structural studies to date[4] have not yet revealed which tautomeric form is bound to the metal ion in the catalytic site of rePON1. All we know that the metal ion in rePON1 is coordinated by five amino acid residues (Glu53, Asn168, Asn224, Asp269, and Asn270) along with the carbonyl oxygen of 2HQ and a water molecule. However, the unique chemistry of Ln^{3+} includes the so-called labile capping bond phenomenon,[46,47] which is often used to explain unusual Ln^{3+} coordination properties during complex formation. This is why the stability and lability of Ln^{3+}-based complexes are extremely dependent on the surrounding environment and geometry around the central trivalent ion, and why the affinities of ion–ligand binding are very difficult to predict or design in advance.

As 2HQ concentrations exceed 250 μM, the emission intensity gradually decreases (Fig. 3A), suggesting a ligand-induced quenching effect. Several possible mechanisms may contribute to this quenching behavior. The fitted binding model indicates the presence of a second, weaker binding event, with a dissociation constant (K_{D2}) of approximately 1000 μM. This lower-affinity interaction may promote non-radiative switch-off processes, ultimately decreasing phosphorescence efficiency.[44]

Our findings demonstrate that varying the [Tb^{3+}] : [Ca^{2+}] ratio affects the emission intensity (Fig. 3B). A strong initial increase in the signal occurs at low Tb^{3+} concentrations, indicating the successful formation of the rePON1 : Tb^{3+} : 2HQ complex. However, as the [Tb^{3+}] : [Ca^{2+}] ratio increases beyond 5 : 1, the emission intensity decreases, suggesting that an excess amount of Tb^{3+} destabilizes the complex. This trend is consistent with observations made at pH 8.0 (Fig. SI2B†), where similar quenching behavior was detected at elevated Tb^{3+} concentrations. To better understand this behavior, the data were again fitted using the 1 : 1 and 1 : 2 mixed binding model.[44]

This binding model explains the observed trend in emission intensity. The initial increase in intensity correlates with the formation of the rePON1 : Tb^{3+} : 2HQ complex, during which the first Tb^{3+} binding event facilitates efficient ligand-to-metal energy transfer. However, the decreased intensity at higher [Tb^{3+}] : [Ca^{2+}] ratios suggests that an excess amount of Tb^{3+} leads to unfavorable interactions, which could be attributed to three possibilities: (i) competition between Tb^{3+} ions for other binding sites on rePON1, leading to suboptimal coordination environments, as lanthanide ions can form complexes with N- and S-containing donor-type ligands;[48] (ii) precipitation or aggregation of the rePON1 : Tb^{3+} complex at high concentrations, which could result in non-emissive species; and (iii) increased non-radiative relaxation pathways, which may outcompete emission under these conditions.

rePON1-dependent formation of the rePON1 : Tb^{3+} : 2HQ complex

Our working model for the formation of the phosphorescent rePON1 : Tb^{3+} : 2HQ complex is based on the specific intramolecular coordination of Tb^{3+} and 2HQ within the active site of rePON1. It is possible that the observed signal could also be the result of potential dimeric emissive species, such as rePON1 : Tb_2^{3+} : 2HQ (where a single 2HQ ligand transfers energy to two Tb^{3+} ions) or rePON1 : Tb^{3+} : $2HQ_2$ (where two 2HQ ligands transfer energy to one Tb^{3+} ion). In this case, the phosphorescence would not be linearly dependent on the rePON1 concentration due to a shift in equilibrium between the monomeric and dimeric states.

To rule out this possibility and assess the potential of phosphorescence spectroscopy for quantitative detection of rePON1, emission spectra were obtained for a series of rePON1 dilutions in the presence of fixed concentrations of Tb^{3+} and 2HQ. Fig. 4 presents the relationship between the emission intensity (peak area and peak height of the emission signal intensity at 545 nm) and the rePON1 concentration.

Both the peak area and the peak height of emission signal intensity exhibit a strong linear relationship with the rePON1 concentration over the tested range. Fitted linear regression demonstrated high accuracy and reproducibility of the emission signal for rePON1 quantification. Additionally, similar linear relationships between the rePON1 concentration and both the peak area and the peak height of emission signal intensity were observed at pH 8.0 (Fig. SI3†). The linearity observed in this concentration range suggests that under these conditions, the formation of the rePON1 : Tb^{3+} : 2HQ complex follows a predictable stoichiometric relationship, with a direct

Open Access Article. Published on 17 July 2025. Downloaded on 11/16/2025 12:52:30 AM.
This article is licensed under a Creative Commons Attribution-NonCommercial 3.0 Unported Licence.

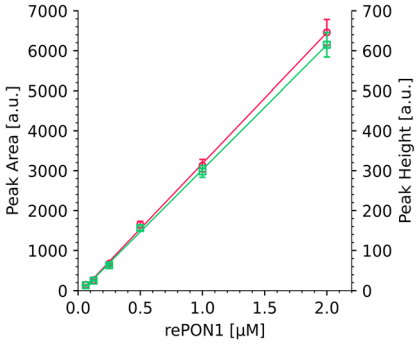

Fig. 4 rePON1-dependent formation of the rePON1 : Tb^{3+} : 2HQ complex. The peak areas (red circles) and peak heights (green squares) of emission signal intensity at 545 nm were plotted against different rePON1 concentrations (0.062–2.0 μM), while maintaining Tb^{3+} and 2HQ concentrations fixed at 50 μM and 400 μM, respectively. The data exhibit a strong linear relationship, with goodness-of-fit R^2 values of 0.9993 for the peak area and 0.9994 for the peak height.

correlation between the rePON1 concentration and the emission intensity.

The high linearity of the calibration curve confirms the suitability of this method for quantitative analysis of PON1. Using the emission peak area provides higher sensitivity, as it integrates the full emission spectrum, whereas the peak height may be less susceptible to spectral broadening or minor fluctuations in emission intensity. Additionally, the absence of signal saturation within this concentration range indicates that energy transfer from 2HQ to Tb^{3+} is still efficient and unaffected by self-quenching or non-radiative relaxation pathways.

Stability of the rePON1 : Tb^{3+} : 2HQ complex under different pH/buffer conditions

To evaluate the long-term stability of the rePON1 : Tb^{3+} : 2HQ complex, the phosphorescence signal was monitored at 545 nm (emission) and 351 nm (excitation) for 600 min in different buffer systems at different pH values. The results (Fig. SI4†) demonstrate that both the buffer composition and pH play a crucial role in complex stability, affecting both the initial emission intensity and the rate of its decay over time.

The stability of the rePON1 : Tb^{3+} : 2HQ complex depended on pH. The most rapid time-dependent decay in emission intensity was observed in bis-tris-propane buffer at pH 6.5 (Fig. SI4†), indicating that the rePON1 : Tb^{3+} : 2HQ complex is unstable under mildly acidic conditions. The sharp decrease in emission intensity suggests that protein aggregation may have occurred. This is consistent with the theoretically calculated isoelectric point of rePON1, *i.e.*, approximately pH 5.0, as approaching this point decreases protein solubility and promotes aggregation. In contrast, bis-tris-propane at pH 7.4 and pH 8.0 exhibited improved complex stability. Although the complex initially displayed slightly higher emission intensity at pH 7.4 compared to pH 8.0, a constant decrease in intensity was observed over time. These observations suggest that although both pH conditions support complex formation, pH 8.0 offers a more favorable environment for maintaining emission intensity over extended periods.

The stability of the rePON1 : Tb^{3+} : 2HQ complex also depends on buffer composition. When comparing different buffer systems at neutral to basic pH, HEPES at pH 7.4 and pH 8.0 exhibited moderate stability, with signal intensity stabilizing after approximately 1 h (Fig. SI4†). This suggests that HEPES may offer stabilizing interactions; however, the overall emission intensity was lower than that observed in bis-tris-propane buffer. The lowest initial emission intensity was observed in tris buffer at pH 8.0, despite showing similar long-term stability to HEPES. These results indicate that the buffer composition affects both the initial emission signal and the overall phosphorescence efficiency. As expected, no emission was detected in phosphate buffer (data not shown), likely due to the strong complexation of Tb^{3+} ions by phosphate groups, which reduces the availability of free terbium ions for supramolecular rePON1 : Tb^{3+} : 2HQ complex formation.

Several factors may have contributed to the observed pH- and buffer-dependent stability. (i) Protonation effects at lower pH may interfere with Tb^{3+} and 2HQ binding to rePON1, leading to a low initial intensity and rapid signal decay at pH 6.5. (ii) Structural rearrangements in rePON1 at different pH levels may modify Tb^{3+} accessibility, influencing the efficiency of ligand-to-metal energy transfer. (iii) The sharp decrease in intensity suggests that protein aggregation may have occurred, leading to the formation of non-emissive species.

Additionally, the thermal stability of rePON1 in the presence of increasing Tb^{3+} concentrations was assessed using nano-differential scanning fluorimetry in 20 mM bis-tris-propane at pH 7.4 and 8.0. The inflection temperature (T_i) decreased with increasing Tb^{3+} concentrations, indicating destabilization of the protein (Fig. SI5A†). The most pronounced shift in T_i occurred between 0 and 100 μM Tb^{3+}, with smaller changes at higher concentrations, suggesting a saturable, destabilizing effect. Similar trends were observed at pH 8.0 (Fig. SI5B†). Although one might expect that the replacement of divalent Ca^{2+} by trivalent Tb^{3+} would result in stronger coordination and increased protein stability, the opposite effect was observed. The destabilization of rePON1 in the presence of Tb^{3+} likely reflects the disruption of the structural integrity of one or both Ca^{2+}-binding sites (catalytic and structural). Given the strong coordination properties of Tb^{3+}, its substitution with Ca^{2+} may induce localized rigidity or conformational strain, ultimately compromising the global folding of the protein.

Crystal structure of the rePON1 : Tb^{3+} : 2HQ complex

We utilized the recombinant rePON1-G2E6 variant, as its crystal structure has previously been determined in a complex with the well-characterized competitive inhibitor 2HQ (PDB 3SRG).[4] We aimed to determine whether Tb^{3+} can substitute Ca^{2+} ions and whether this substitution affects the overall structure of rePON1. The crystal structure of the rePON1 : Tb^{3+} : 2HQ complex (PDB 9R0Q) was determined at a

 This journal is © The Royal Society of Chemistry 2025

Open Access Article. Published on 17 July 2025. Downloaded on 11/16/2025 12:52:30 AM.
This article is licensed under a Creative Commons Attribution-NonCommercial 3.0 Unported Licence.

resolution of 2.35 Å using molecular replacement with the 1V04 structure as a search model. The crystals belonged to the space group *C*422, containing one molecule per asymmetric unit, such as the 1V04 structure.[21]

Positions of Tb^{3+} were determined using an anomalous difference map (Fig. 5A, magenta mesh contoured at 4.9 σ), and it revealed the partial substitution of Ca^{2+} by Tb^{3+} at both Ca^{2+}-binding sites. The refined occupancy of Tb^{3+} was estimated at ~47% and ~5% at the catalytic and structural sites, respectively, which are separated by ~7.6 Å. The remaining occupancy is attributed to residual Ca^{2+}, which was present in the crystallization solution.

At the catalytic site, metal ions are coordinated by five protein residues (Glu53, Asn168, Asn224, Asp269, and Asn270) along with a water molecule and an oxygen atom from 2HQ (Fig. 5B), forming a slightly distorted pentagonal bipyramidal geometry typical of Ca^{2+}-binding proteins. In contrast, the Tb^{3+} ion at the structural site is coordinated by Asp54, Asp169, the backbone carbonyl of Ile117, and three water molecules, which are stabilized by hydrogen bonding to surrounding residues.

Structural comparisons (Fig. 5B) between the Tb^{3+}- (PDB 9R0Q) and Ca^{2+}-bound (PDB 3SRG) structures revealed high overall similarity, with C_α RMSD values of 0.335 Å and 0.352 Å for backbone atoms and 0.646 Å when all fully modelled residues were included. These values are consistent with the expected RMSD values for independently determined structures of the same protein.[49] The geometries at both the catalytic (C) and structural (S) metal-binding sites were nearly identical.[4] This indicates that Tb^{3+} incorporation at the catalytic site does not cause significant structural rearrangement and the overall protein fold is preserved upon partial Ca^{2+} substitution.

However, the negligible occupancy of Tb^{3+} at the structural site highlights distinct differences in accessibility and substitution dynamics between the two sites. Although the structural site is believed to have a higher affinity for Ca^{2+} than the catalytic site, this alone does not account for its resistance to substitution. Two major factors likely contribute to the limited substitution of Ca^{2+} by Tb^{3+} at the structural binding site. First, Ca^{2+} was present in excess (~1.8 molar equivalents) during crystallization, favoring its re-binding to the high-affinity site during equilibration. Second, the local coordination environment (comprising two aspartate residues, a backbone carbonyl, and three tightly bound water molecules) is in a narrow cleft of the six-bladed β-propeller (Fig. SI6†). This geometrically constrained and inaccessible pocket likely restricts ion exchange, effectively "trapping" native Ca^{2+} and limiting displacement by Tb^{3+}.

This interpretation is further supported by differences in desolvation kinetics between the two ions.[50,51] Trivalent ions such as Tb^{3+} exhibit significantly slower desolvation rates compared to the almost instantaneous desolvation of Ca^{2+}. For Tb^{3+} to occupy the structural site, Ca^{2+} must first vacate the pocket, and Tb^{3+} must shed its hydration shell—a process that is energetically unfavorable for trivalent lanthanide ions. Moreover, the desolvation and binding of Tb^{3+} must occur faster than the re-binding of Ca^{2+}, which is unlikely given the rapid water exchange kinetics and favorable coordination of Ca^{2+} within this high-affinity site. In addition, the relatively lower molar ratio of Tb^{3+} and its potential complexation with bis-tris-propane[52] in the crystallization buffer may further diminish the pool of free Tb^{3+} ions available for substitution. Thus, under these conditions, the probability of a single Tb^{3+} ion outcompeting the Ca^{2+} ion for access to the buried site is low, explaining the low Tb^{3+} occupancy observed.

Interestingly, the detection of low but measurable Tb^{3+} occupancy at the structural binding site (~5%) suggests that occasional conformational fluctuations or transient breathing motions may briefly expose the site to solvent, thereby permitting rare substitution events.[53] This observation may highlight a dynamic interplay between thermodynamic favorability and kinetic accessibility, where the stronger coordination potential of Tb^{3+} is counterbalanced by the limited accessibility of the structural binding site and the kinetic advantage of Ca^{2+} under the given conditions.

In attempts to increase Tb^{3+} occupancy, rePON1 was dialyzed into Tb^{3+}-only buffer (20 mM HEPES, pH 8.0, 0.03% *n*-dodecyl β-D-maltoside); however, this led to poor crystallization or crystals with inadequate diffraction quality. It is also possible that full substitution of Ca^{2+} with Tb^{3+} compromises crystallization by destabilizing the protein and/or altering crystal contacts. These experimental observations suggest that complete metal ion substitution may disrupt proper protein folding or packing, highlighting the delicate balance between functional metal coordination and structural integrity.

In contrast, the catalytic site is more solvent exposed, with a more dynamic coordination environment that includes both protein ligands and solvent-accessible components (*e.g.*, water and 2HQ).[4] These features likely promote more efficient exchange, as reflected in the higher Tb^{3+} occupancy at this site.

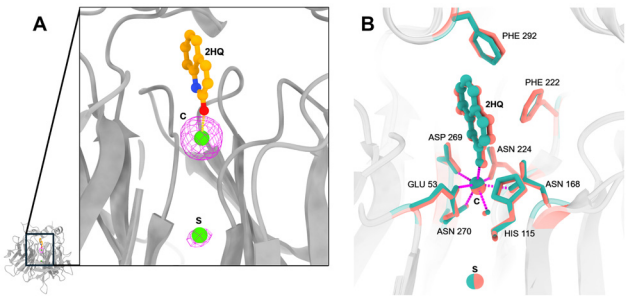

Fig. 5 (A) Ribbon representation of rePON1 (PDB 9R0Q) showing the bound ligand 2-hydroxyquinoline (2HQ, orange) and two metal-binding sites, catalytic (C) and structural (S), each occupied by a green sphere (representing Ca^{2+} or Tb^{3+}). The anomalous signal for Tb^{3+} is shown as a magenta mesh (contoured at 4.9 σ). (B) Structural alignment between Tb^{3+}-bound rePON1 (PDB 9R0Q, teal) and Ca^{2+}-bound rePON1 (PDB 3SRG, coral), highlighting conservation in the active site architecture. Close-up view of the catalytic binding site (C), illustrating key residues involved in metal coordination (Glu53, Asn168, Asn224, Asp269, and Asn270) and ligand stabilization (His115, Phe222, and Phe292). Catalytic (C) and structural (S) metal-binding sites are indicated as spheres.

Open Access Article. Published on 17 July 2025. Downloaded on 11/16/2025 12:52:30 AM.
This article is licensed under a Creative Commons Attribution-NonCommercial 3.0 Unported Licence.

Finally, the 2HQ ligand was resolved in the electron density, with an estimated occupancy of 82%, and bound at the same site observed in the Ca^{2+}-bound structure (PDB ID: 3SRG). Notably, residues 71–81, which form the so-called "active-site loop", were well-ordered and adopted the closed conformation characteristic of ligand-bound states, consistent with the 3SRG structure. These findings indicate that 2HQ binding (although with lower affinity) is not perturbed by Tb^{3+} substitution at the catalytic site and the overall ligand-binding mode and catalytic-site conformation are preserved in the Tb^{3+}-substituted complex.

Conclusions

Luminescent lanthanide ions exhibit unique spectroscopic properties, including long-lived excited states that allow phosphorescence experiments, and the elimination of background fluorescence associated with biological media, as well as metal-specific and characteristic narrow emission bands in comparison with typical organic fluorophores, which make them attractive for various bioluminescence assays.[54] In this study, we investigated the potential of a self-assembled phosphorescent ternary complex rePON1 : Tb^{3+} : 2HQ for PON1 detection. Specifically, we examined whether substituting native Ca^{2+} with Tb^{3+} in rePON1 alters the enzyme's structure and ligand-binding capacity and whether this can be utilized for phosphorescence-based quantification of PON1 or other metallo-enzymes.

Our results reveal that 2HQ forms a highly emissive ternary complex with rePON1 : Tb^{3+}, exhibiting Tb^{3+}-dependent phosphorescence. The emission intensity of this complex correlated linearly with rePON1 concentration, providing proof of concept for metallo-enzyme quantification independent of its catalytic function. Crystallographic data of the rePON1 : Tb^{3+} : 2HQ complex at 2.35 Å resolution demonstrated that Tb^{3+} substitutes Ca^{2+} at the catalytic site without inducing major structural rearrangements, although negligible Tb^{3+} occupancy was observed at the structural Ca^{2+} site.

Collectively, these findings establish a structural and mechanistic foundation for the use of photoluminescent lanthanide ion complexes in biosensing and quantification of PON1. Future efforts should focus on identifying higher-affinity aromatic ligands for the rePON1 : Tb^{3+} complex, as low-affinity ligands require elevated concentrations that increase the risk of self-quenching and decrease signal reliability. Additional structural work targeting complete metal substitution, perhaps through protein engineering or site-directed mutagenesis to modify metal accessibility, could further elucidate the conformational dynamics involved. Finally, adapting this system for the detection of endogenous PON1 in complex biological matrices such as human serum represents a critical step toward clinical translation and real-world diagnostic applications, especially for independent PON1 concentration quantification which would upgrade the usual PON1 activity measurements.

Altogether, this work not only advances our understanding of metal ion modulation in rePON1 but also establishes a novel, phosphorescence-based platform for selective, activity-independent detection of this and other clinically important metallo-enzymes, laying the groundwork for future biosensing and diagnostic innovations.

Author contributions

Janez Smerkolj: conceptualization, data curation, formal analysis, investigation, methodology, visualization, and writing – original draft; Miha Bahun: methodology, supervision, and writing – review & editing; Nataša Poklar Ulrih: supervision and writing – review & editing; Aljoša Bavec: methodology, supervision, and writing – review & editing; Miha Pavšič: data curation, formal analysis, investigation, methodology, supervision, and writing – review & editing; Marko Goličnik: conceptualization, formal analysis, investigation, methodology, supervision, writing – original draft, and writing – review & editing. All authors read and contributed to the critical review of the manuscript for intellectual content and approved the submission for publication.

Conflicts of interest

There are no conflicts to declare.

Data availability

All the relevant experimental data have been provided in the manuscript and the ESI†. Crystallographic data for the ternary complex rePON1 : Tb^{3+} : 2HQ have been deposited at the RCSB Protein Data Bank (RCSB PBD) under identification number 9R0Q.

Acknowledgements

This work was supported by the Slovenian Research Agency young researcher grant (No. 55728, Janez Smerkolj) and Slovenian Research Agency research programs P1-0170 (Janez Smerkolj, Aljoša Bavec, and Marko Goličnik), P1-0140 (Miha Pavšič), and P4-0121 (Miha Bahun and Nataša Poklar Ulrih).

The authors thank Elettra Synchrotron, Italy, for the beamtime and support, with special thanks to Nicola Demitri and Raghurama Prabhakara Hegde from the XRD2 beamline at the Elettra Synchrotron, Italy, for their kind assistance and excellent support during diffraction characterization and data collection (proposal ID 20240549).

We thank Eva Lasič (PhD) for editing and reviewing a draft of this manuscript.

Molecular graphics and analyses were performed using UCSF ChimeraX, developed by the Resource for Biocomputing, Visualization, and Informatics at the University of California,

 This journal is © The Royal Society of Chemistry 2025

Open Access Article. Published on 17 July 2025. Downloaded on 11/16/2025 12:52:30 AM.
This article is licensed under a Creative Commons Attribution-NonCommercial 3.0 Unported Licence.

San Francisco, with support from the National Institutes of Health R01-GM129325 and the Office of Cyber Infrastructure and Computational Biology, National Institute of Allergy and Infectious Diseases. The graphical abstract was created in https://BioRender.com.

References

1 A. Taler-Verčič, M. Goličnik and A. Bavec, The structure and function of paraoxonase-1 and its comparison to paraoxonase-2 and-3, *Molecules*, 2020, **25**(24), 5980, DOI: 10.3390/molecules25245980.

2 M. Mackness and B. Mackness, Human paraoxonase-1 (PON1): Gene structure and expression, promiscuous activities and multiple physiological roles, *Gene*, 2015, **567**(1), 12–21, DOI: 10.1016/j.gene.2015.04.088.

3 X. Gu, Y. Huang, B. S. Levison, *et al.*, Identification of critical paraoxonase 1 residues involved in high density lipoprotein interaction, *J. Biol. Chem.*, 2016, **291**(4), 1890–1904, DOI: 10.1074/jbc.M115.678334.

4 M. Ben-David, M. Elias, J. J. Filippi, *et al.*, Catalytic versatility and backups in enzyme active sites: The case of serum paraoxonase 1, *J. Mol. Biol.*, 2012, **418**(3–4), 181–196, DOI: 10.1016/j.jmb.2012.02.042.

5 M. Ben-David, J. L. Sussman, C. I. Maxwell, *et al.*, Catalytic stimulation by restrained active-site floppiness—The case of high density lipoprotein-bound serum paraoxonase-1, *J. Mol. Biol.*, 2015, **427**(6), 1359–1374, DOI: 10.1016/j.jmb.2015.01.013.

6 D. Blaha-Nelson, D. M. Krüger, K. Szeler, *et al.*, Active site hydrophobicity and the convergent evolution of paraoxonase activity in structurally divergent enzymes: The case of serum paraoxonase 1, *J. Am. Chem. Soc.*, 2017, **139**(3), 1155–1167, DOI: 10.1021/jacs.6b10801.

7 M. Ben-David, M. Soskine, A. Dubovetskyi, *et al.*, Enzyme evolution: An epistatic ratchet versus a smooth reversible transition, *Mol. Biol. Evol.*, 2020, **37**(4), 1133–1147, DOI: 10.1093/molbev/msz298.

8 J. F. Teiber, J. Xiao, G. L. Kramer, *et al.*, Identification of biologically active δ-lactone eicosanoids as paraoxonase substrates, *Biochem. Biophys. Res. Commun.*, 2018, **505**(1), 87–92, DOI: 10.1016/j.bbrc.2018.09.083.

9 O. Khersonsky and D. S. Tawfik, Structure-reactivity studies of serum paraoxonase PON1 suggest that its native activity is lactonase, *Biochemistry*, 2005, **44**(16), 6371–6382, DOI: 10.1021/bi047440d.

10 H. Soran, J. D. Schofield and P. N. Durrington, Antioxidant properties of HDL, *Front. Pharmacol.*, 2015, **6**, 222, DOI: 10.3389/fphar.2015.00222.

11 M. Aviram, M. Rosenblat, C. L. Bisgaier, *et al.*, Paraoxonase inhibits high-density lipoprotein oxidation and preserves its functions A possible peroxidative role for paraoxonase, *J. Clin. Invest.*, 1998, **101**(8), 1581–1590, DOI: 10.1172/JCI1649.

12 P. Durrington and H. Soran, Paraoxonase 1: evolution of the enzyme and of its role in protecting against atherosclerosis, *Curr. Opin. Lipidol.*, 2024, **35**(4), 171–178, DOI: 10.1097/MOL.0000000000000936.

13 T. Menini and A. Gugliucci, Paraoxonase 1 in neurological disorders, *Redox Rep.*, 2014, **19**(2), 49–58, DOI: 10.1179/1351000213Y.0000000071.

14 B. Petrič, S. Redenšek Trampuž, V. Dolžan, *et al.*, Investigation of paraoxonase-1 genotype and enzyme-kinetic parameters in the context of cognitive impairment in Parkinson's disease, *Antioxidants*, 2023, **12**(2), 399, DOI: 10.3390/antiox12020399.

15 J. Watanabe, K. Kotani and A. Gugliucci, Paraoxonase 1 and chronic obstructive pulmonary disease: A meta-analysis, *Antioxidants*, 2021, **10**(12), 1891, DOI: 10.3390/antiox10121891.

16 E. C. Samouilidou, A. Liaouri, V. Kostopoulos, *et al.*, The importance of paraoxonase 1 activity in chronic kidney disease, *Renal Failure*, 2024, **46**(2), 2376930, DOI: 10.1080/0886022X.2024.2376930.

17 J. Camps, S. Iftimie, M. Arenas, *et al.*, Paraoxonase-1: How a xenobiotic detoxifying enzyme has become an actor in the pathophysiology of infectious diseases and cancer, *Chem.-Biol. Interact.*, 2023, **380**, 110553, DOI: 10.1016/j.cbi.2023.110553.

18 D. Denimal, Antioxidant and anti-inflammatory functions of high-density lipoprotein in type 1 and type 2 diabetes, *Antioxidants*, 2024, **13**(1), 57, DOI: 10.3390/antiox13010057.

19 E. H. Van Den Berg, E. G. Gruppen, R. W. James, *et al.*, Serum paraoxonase 1 activity is paradoxically maintained in nonalcoholic fatty liver disease despite low HDL cholesterol, *J. Lipid Res.*, 2019, **60**(1), 168–175, DOI: 10.1194/jlr.P088997.

20 A. Aharoni, L. Gaidukov, S. Yagur, *et al.*, Directed evolution of mammalian paraoxonases PON1 and PON3 for bacterial expression and catalytic specialization, *Proc. Natl. Acad. Sci. U. S. A.*, 2004, **101**(2), 482–487, DOI: 10.1073/pnas.2536901100.

21 M. Harel, A. Aharoni, L. Gaidukov, *et al.*, Structure and evolution of the serum paraoxonase family of detoxifying and anti-atherosclerotic enzymes, *Nat. Struct. Mol. Biol.*, 2004, **11**(5), 412–419, DOI: 10.1038/nsmb767.

22 M. Ben-David, G. Wieczorek, M. Elias, *et al.*, Catalytic metal ion rearrangements underline promiscuity and evolvability of a metalloenzyme, *J. Mol. Biol.*, 2013, **425**(6), 1028–1038, DOI: 10.1016/j.jmb.2013.01.009.

23 C. L. Kuo and B. N. La Du, Calcium binding by human and rabbit serum paraoxonases. Structural stability and enzymatic activity, *Drug Metab. Dispos.*, 1998, **26**(7), 653–660.

24 D. Josse, W. Xie, F. Renault, *et al.*, Identification of residues essential for human paraoxonase (PON1) arylesterase/organophosphatase activities, *Biochemistry*, 1999, **38**(9), 2816–2825, DOI: 10.1021/bi982281h.

25 A. Pla, L. Rodrigo, A. F. Hernández, *et al.*, Effect of metal ions and calcium on purified PON1 and PON3 from rat

Open Access Article. Published on 17 July 2025. Downloaded on 11/16/2025 12:52:30 AM.
This article is licensed under a Creative Commons Attribution-NonCommercial 3.0 Unported Licence.

liver, *Chem.-Biol. Interact.*, 2007, **167**(1), 63–70, DOI: 10.1016/j.cbi.2007.01.006.

26 J. Debord, J. C. Bollinger, L. Merle, *et al.*, Inhibition of human serum arylesterase by metal chlorides, *J. Inorg. Biochem.*, 2003, **94**(1–2), 1–4, DOI: 10.1016/S0162-0134(02)00627-x.

27 L. G. Costa, T. B. Cole, J. M. Garrick, *et al.*, Metals and paraoxonases, *Adv. Neurobiol.*, 2017, **18**, 85–111, DOI: 10.1007/978-3-319-60189-2_5.

28 E. G. Erdös, C. R. Debay and M. P. Westerman, Arylesterases in blood: effect of calcium and inhibitors, *Biochem. Pharmacol.*, 1960, **5**, 173–186, DOI: 10.1016/0006-2952(60)90061-7.

29 K. Djinovic-Carugo and O. Carugo, Structural biology of the lanthanides - Mining rare earths in the Protein Data Bank, *J. Inorg. Biochem.*, 2015, **143**, 69–76, DOI: 10.1016/j.jinorgbio.2014.12.005.

30 J. C. G. Bünzli and C. Piguet, Taking Advantage of Luminescent Lanthanide Ions, *Chem. Soc. Rev.*, 2005, **34**(12), 1048–1077, DOI: 10.1039/b406082m.

31 J. C. G. Bünzli, Lanthanide luminescence for biomedical analyses and imaging, *Chem. Rev.*, 2010, **110**(5), 2729–2755, DOI: 10.1021/cr900362e.

32 P. R. Selvin and J. E. Hearst, Luminescence energy transfer using a terbium chelate: Improvements on fluorescence energy transfer, *Proc. Natl. Acad. Sci. U. S. A.*, 1994, **91**, 10024–10028, DOI: 10.1073/pnas.91.21.10024.

33 P. Ge and P. R. Selvin, Carbostyril derivatives as antenna molecules for luminescent lanthanide chelates, *Bioconjugate Chem.*, 2004, **15**(5), 1088–1094, DOI: 10.1021/bc049915j.

34 Y. Yang, Z. Zhou, Z. Z. Wei, *et al.*, High anticancer activity and apoptosis- and autophagy-inducing properties of novel lanthanide(iii) complexes bearing 8-hydroxyquinoline-N-oxide and 1,10-phenanthroline, *Dalton Trans.*, 2021, **50**(17), 5828–5834, DOI: 10.1039/d1dt00450f.

35 R. Akbar, M. Baral and B. K. Kanungo, Spectroscopic, photophysical, solution thermodynamics and computational study of europium and terbium complexes with a flexible quinolinol-based symmetric tripodal chelator, *Spectrochim. Acta, Part A*, 2021, **247**, 119124, DOI: 10.1016/j.saa.2020.119124.

36 F. S. Richardson, Terbium(III) and europium(III) ions as luminescent probes and stains for biomolecular systems, *Chem. Rev.*, 1982, **82**(5), 541–552, DOI: 10.1021/cr00051a004.

37 H. Xu, Q. Sun, Z. An, *et al.*, Electroluminescence from europium(III) complexes, *Coord. Chem. Rev.*, 2015, **293–294**, 228–249, DOI: 10.1016/j.ccr.2015.02.018.

38 J. R. Lakowicz, *Principles of Fluorescence Spectroscopy*, 3rd edn, 2006.

39 A. Beeby, I. M. Clarkson, R. S. Dickins, *et al.*, Non-radiative deactivation of the excited states of europium, terbium and ytterbium complexes by proximate energy-matched OH, NH and CH oscillators: An improved luminescence method for establishing solution hydration states, *J. Chem. Soc., Perkin Trans. 2*, 1999, (3), 493–503, DOI: 10.1039/a808692c.

40 S. Zhang, K. Wu and A. D. Sherry, Unusually sharp dependence of water exchange rate versus lanthanide ionic radii for a series of tetraamide complexes, *J. Am. Chem. Soc.*, 2002, **124**(16), 4226–4227, DOI: 10.1021/ja017133k.

41 D. Josse, W. Xie, P. Masson, *et al.*, Tryptophan residue(s) as major components of the human serum paraoxonase active site, *Chem.-Biol. Interact.*, 1999, **119–120**(120), 79–84, DOI: 10.1016/s0009-2797(99)00016-2.

42 X. Deng, X. Chai, C. Wei, *et al.*, Rapid determination of quinoline and 2-hydroxyquinoline in quinoline biodegradation process by tri-wavelength UV/VIS spectroscopy, *Anal. Sci.*, 2011, **27**(5), 493, DOI: 10.2116/analsci.27.493.

43 A. Slodek, M. Filapek, G. Szafraniec, *et al.*, Synthesis, electrochemistry, crystal structures, and optical properties of quinoline derivatives with a 2,2′-bithiophene motif, *Eur. J. Org. Chem.*, 2014, **2014**(24), 5256–5264, DOI: 10.1002/ejoc.201402241.

44 T. Gunnlaugsson, A. J. Harte, J. P. Leonard, *et al.*, The formation of luminescent supramolecular ternary complexes in water: Delayed luminescence sensing of aromatic carboxylates using coordinated unsaturated cationic heptadentate lanthanide ion complexes, *Supramol. Chem.*, 2003, **15**(7–8), 505–519, DOI: 10.1080/10610270310001605106.

45 M. R. Nimlos, D. F. Kelley and E. R. Bernstein, Spectroscopy and structure of 2-hydroxyqulnoline, *J. Phys. Chem.*, 1987, **91**, 6610–6614, DOI: 10.1021/j100311a011.

46 A. Rodríguez-Rodríguez, M. Regueiro-Figueroa, D. Esteban-Gómez, *et al.*, Definition of the labile capping bond effect in lanthanide complexes, *Chem. – Eur. J.*, 2017, **23**(5), 1110–1117, DOI: 10.1002/chem.201604390.

47 A. Lemieux and M. Dolg, Labile capping bonds in lanthanide(III) complexes: shorter and weaker, *J. Phys. Chem.*, 2014, **119**(4), 29, DOI: 10.1021/jp511043c.

48 S. Li, S. Jansone-Popova and D. E. Jiang, Insights into coordination and ligand trends of lanthanide complexes from the Cambridge Structural Database, *Sci. Rep.*, 2024, **14**, 11301, DOI: 10.1038/s41598-024-62074-3.

49 O. Carugo, How root-mean-square distance (r.m.s.d.) values depend on the resolution of protein structures that are compared, *J. Appl. Crystallogr.*, 2003, (36), 125–128, DOI: 10.1107/S0021889802020502.

50 T. Dudev and C. Lim, Competition among metal ions for protein binding sites: Determinants of metal ion selectivity in proteins, *Chem. Rev.*, 2014, **114**(1), 538–556, DOI: 10.1021/cr4004665.

51 H. Diebler, M. Eigen, G. Ilgenfritz, *et al.*, Kinetics and mechanism of reactions of main group metal ions with biological carriers, *Pure Appl. Chem.*, 2009, **20**(1), 93–116, DOI: 10.1351/pac196920010093.

52 P. Gómez-Tagle and A. K. Yatsimirsky, Phosphodiester hydrolysis by lanthanide complexes of bis-Tris propane, *Inorg. Chem.*, 2001, **40**(15), 3786–3796, DOI: 10.1021/ic0010205.

53 S. Aime, A. Barge, M. Botta, *et al.*, Direct NMR spectroscopic observation of a lanthanide-coordinated water mole-

 This journal is © The Royal Society of Chemistry 2025

Open Access Article. Published on 17 July 2025. Downloaded on 11/16/2025 12:52:30 AM.
This article is licensed under a Creative Commons Attribution-NonCommercial 3.0 Unported Licence.

cule whose exchange rate is dependent on the conformation of the complexes, *Angew. Chem., Int. Ed.*, 1998, **37**(19), 2673–2675, DOI: 10.1002/(SICI)1521-3773(19981016)37:19<2673::AID-ANIE2673>3.0.CO;2-%23.

54 R. Sanchez-Fernandez, I. Obregon-Gomez, A. Sarmiento, *et al.*, Luminescent lanthanide metallopeptides for biomolecule sensing and cellular imaging, *Chem. Commun.*, 2024, **60**(87), 12650–12661, DOI: 10.1039/D4CC03205E.